Comparison of Impedance Eduction Test Rigs with Different Boundary-Layer Profiles

Comparison of Impedance Eduction Test Rigs with Different Boundary-Layer Profiles

Nicolas T. Quintino,* Lucas A. Bonomo,† and Julio A. Cordioli‡
Federal University of Santa Catarina, 88040-900 Florianópolis, Brazil
Michael G. Jones,§ Brian M. Howerton,¶ and Douglas M. Nark**
NASA Langley Research Center, Hampton, Virginia 23681
and
Francesco Avallone††
Politecnico di Torino, 10129 Turin, Italy

https://doi.org/10.2514/1.J065173

The experimental characterization of acoustic liners has garnered significant attention within the research community. Typically, such characterization involves measuring the acoustic impedance of liners using various techniques under conditions similar to those found in turbofan engines. This study aims to offer a comparative analysis of educed acoustic impedance for two liner samples, manufactured by the same provider and tested in the UFSC Impedance Test Rig and the NASA GFIT. Leveraging the distinct geometries of these test rigs, the investigation considers the impact of different grazing flow profiles in terms of the boundary-layer displacement thickness on the educed impedance. Notably, impedance measurements exhibit congruent outcomes in the absence of grazing flow but diverge in terms of resistance values when grazing flow is present, with the UFSC Impedance Test Rig consistently indicating higher values. The postprocessing algorithms of both institutions are uniform. In addition, a comparison involving a semiempirical predictive model has been conducted. The findings suggest that the observed disparities relate to the grazing flow boundary-layer profile. In summary, it is important to report both the mean flow Mach number and the displacement thickness to enable proper comparison between impedances educed from data acquired in different test rigs.

Nomenclature

A	=	modal amplitude
A_a	=	active chamber area
A_t	=	total chamber area
C_d	=	discharge coefficient
c_0	=	speed of sound
d	=	perforate plate hole diameter
d_c	=	chamber dimension (length)
h	=	cavity height
i	=	imaginary unit
J	=	Bessel function
k	=	free-field wavenumber
k_s	=	wavenumber of viscous Stokes wave
k_x	=	transverse wavenumber
k_z	=	axial wavenumber
M	=	bulk Mach number
N	=	number of microphones
P_n	=	Prandtl number
p	=	complex acoustic pressure
R_{cm}	=	normalized grazing flow-induced acoustic resistance
S_m	=	nonlinear mass reactance
S_r	=	nonlinear resistance slope
t	=	facesheet thickness
U_0	=	root-mean-squared acoustic particle velocity
u	=	acoustic particle velocity
w	=	measurement noise
x	=	transverse coordinate
Z	=	acoustic impedance
Z_0	=	air characteristic impedance
Z_b	=	core impedance considering blockage
Z_c	=	empty chamber characteristic impedance
Z_{of}	=	perforate plate impedance
z	=	axial coordinate
Γ	=	propagation constant
γ	=	heat capacity ratio
Δz	=	distance between microphones
ϵd	=	mass end correction
μ	=	air viscosity
ρ_0	=	air density
σ	=	open area ratio
ψ	=	mode shape
ω	=	angular frequency

Presented as Paper 2023-3346 at the AIAA Aviation Forum 2023, San Diego, CA, June 12–16, 2023; received 26 November 2024; accepted for publication 2 April 2025; published online Open Access 18 June 2025.

*Engineering Research Fellow, Department of Mechanical Engineering; nicolas.quintino@lva.ufsc.br. Member AIAA.

†Ph.D. Student, Department of Mechanical Engineering; lucas.bonomo@lva.ufsc.br. Member AIAA (Corresponding Author).

‡Associate Professor, Department of Mechanical Engineering; julio.cordioli@ufsc.br. Member AIAA.

§Senior Research Scientist, Research Directorate, Applied Acoustics Branch. Associate Fellow AIAA.

¶Research Scientist, Research Directorate, Applied Acoustics Branch; brian.m.howerton@nasa.gov. Senior Member AIAA.

**Senior Research Scientist, Research Directorate, Applied Acoustics Branch. Associate Fellow AIAA.

††Full Professor, Department of Mechanical and Aerospace Engineering; francesco.avallone@polito.it. Member AIAA.

All relevant data enclosured in this work is available at https://doi.org/10.5281/zenodo.15195587.

I. Introduction

ACOUSTIC liners are passive devices typically applied to turbofan nacelles to attenuate fan noise. A liner is commonly composed of a honeycomb structure covered with a perforated plate and backed with a rigid panel, with the liner usually being tuned so that it attenuates the frequency range near the fundamental fan blade passage frequency (BPF) or its harmonics. Recent aircraft engine

designs trend toward larger-diameter engines with increased bypass ratios. In order to limit drag and fuel burn, the nacelles of these new engines tend to have a smaller aspect ratio, between length and diameter, and thinner walls [1]. For the same fan tip speed, a larger diameter lowers the BPF, which would typically require the liners to be thicker. However, thinner walls reduce the volume available for the installation of acoustic liners. To address these challenges, significant efforts are being made to design novel liner concepts that can achieve similar attenuation with reduced dimensions [2]. However, the proper characterization of liners in the presence of high sound pressure levels (SPLs) and grazing flow, as well as the physics involved in sound attenuation by the liner, remain topics of discussion within the community [3–5].

Typically, an acoustic liner is characterized by its acoustic impedance, which is known to depend on both liner geometry (cavity height, percentage of open area, hole diameters, etc.) and operational conditions, such as grazing flow speed and SPL [6–10]. Consequently, this liner evaluation needs to be conducted under conditions resembling the nacelle environment as closely as possible. To achieve this, a set of impedance eduction [11,12] techniques has been proposed with the primary objective of accurately characterizing acoustic liners in realistic scenarios. The fundamental approach involves placing an acoustic liner sample within an instrumented duct where a grazing flow is combined with an acoustic field. Subsequently, the liner's acoustic impedance is determined through measurements of the acoustic field within the test rig.

Despite the substantial number of published articles on impedance eduction techniques, there is a scarcity of direct comparisons between various test rigs and eduction methodologies using identical liner samples. Recently, the International Forum for Aviation Research (IFAR) initiated a collaborative project with the objective of addressing this gap [3,13]. The first challenge under the IFAR liner topic involved collecting data from multiple test rigs utilizing simple liner configurations feasible for construction using 3D-printing technology. However, the precision and surface finishing of 3D-printing equipment can vary significantly, raising concerns about sample uniformity due to anticipated manufacturing process disparities [3]. Additionally, differences in test rig geometries and flow supply systems likely result in distinct flow profiles at each rig, aspects that were not assessed in the aforementioned study. It is noteworthy that the work by Kooi and Sarin [6] suggested a potential strong correlation between the liner's local impedance and the flow profile across the perforated sheet.

The primary objective of this study is to perform a comprehensive comparison between impedance eduction results acquired from two distinct test rigs, using a pair of identical 3D-printed samples manufactured consecutively by the same vendor employing the same equipment. The two test rigs in question are the impedance test rigs located at the Federal University of Santa Catarina (UFSC) and the NASA Langley Research Center Grazing Flow Impedance Tube (GFIT). The use of the same manufacturer and equipment for sample production is expected to yield highly similar test samples, differing primarily in overall dimensions due to the unique rig geometries. This study also assesses the impact on the measurements of the different flow profiles between the two facilities. For the purpose of this comparison, tests are conducted for two different conditions: i) same average Mach number and ii) same centerline Mach number. Both institutions employ a direct eduction method based on Prony's algorithm to evaluate liner impedance [10,14]. Additionally, inverse eduction methods are employed: UFSC utilizes the mode-matching method [4], while NASA employs the convected Helmholtz equation method [15]. To ensure consistency across algorithm implementation, raw data is exchanged between the institutions, allowing each to process data obtained from the other test rig. Lastly, a comprehensive analysis of the results is presented, encompassing a comparison of the educed impedance with a semiempirical model of the liner impedance.

The rest of the paper is structured as follows: Section II outlines the impedance eduction techniques employed in this study, offering a comprehensive depiction of both test rigs. Furthermore, a description of the Goodrich semiempirical liner impedance model ([16]), which will be utilized in subsequent analyses, is provided. Section III presents the main results and discussions. Finally, the main conclusions are outlined in Sec. IV.

II. Experimental Setup and Eduction Methods

A. Impedance Eduction

For the purpose of this work, both test rigs can be simplified as a bidimensional duct, as schematically depicted in Fig. 1. Assuming temporal dependence in the form of $\exp(\mathrm{i}\omega t)$, acoustic propagation can be modeled by the convected Helmholtz equation given by

$$\left(\mathrm{i}k + M\frac{\partial}{\partial z}\right)^2 p - \frac{\partial^2 p}{\partial x^2} - \frac{\partial^2 p}{\partial z^2} = 0 \tag{1}$$

where p is the complex acoustic pressure, $k = \omega/c_0$ is the free-field wavenumber, ω is the angular frequency, c_0 is the speed of sound, $M = U/c_0$ is the flow Mach number, and U is the flow velocity, with Cartesian coordinates x and z in the transverse and axial directions, respectively.

The solution to Eq. (1) is given by a sum of downstream and upstream acoustic propagating modes:

$$p(x,z) = \sum_{n=1}^{\infty} A_n^+ \psi_n^+(x) \exp(-\mathrm{i}k_{z,n}^+ z) + \sum_{n=1}^{\infty} A_n^- \psi_n^-(x) \exp(-\mathrm{i}k_{z,n}^- z) \tag{2}$$

where $A_n^{\pm}$ are the modal amplitudes, $\psi_n^{\pm}(x)$ are the mode shapes, $k_{z,n}^{\pm}$ are the axial wavenumbers, n is the mode index, and $+$ and $-$ denote downstream and upstream propagating waves, respectively. In the lined section of the duct, the bottom wall ($x = 0$) is lined with a wall impedance Z, while the upper wall ($x = H$, where H is the duct height) is rigid. The normal component of the acoustic particle velocity vanishes in the presence of a rigid wall, such that the boundary condition is given by

$$\frac{\partial p}{\partial x} = 0, \text{ at } x = H \tag{3}$$

For lined walls, the refraction in the boundary layer is taken into account by means of the Ingard–Myers boundary condition [17,18], leading to

$$\frac{\partial p}{\partial x} = \frac{Z_0}{\mathrm{i}kZ}\left(\mathrm{i}k + M\frac{\partial}{\partial z}\right)^2 p, \quad \text{at } x = 0 \tag{4}$$

where $Z_0 = \rho_0 c_0$ is the air characteristic impedance and ρ_0 is the air density. These boundary conditions applied to Eq. (2) lead to the eigenvalue problem

$$k_{x,n}\tan(k_{x,n}H) - \frac{Z_0}{\mathrm{i}kZ}(\mathrm{i}k - \mathrm{i}Mk_{z,n})^2 = 0 \tag{5}$$

where $k_{x,n}$ are the transverse wavenumbers, and the dispersion relation is given by

$$k_{x,n}^2 = (k - Mk_{z,n})^2 - k_{z,n}^2 \tag{6}$$

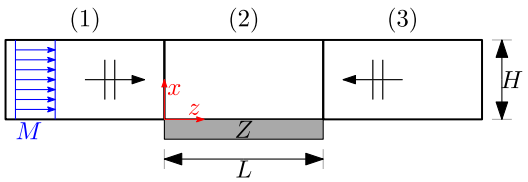

Fig. 1 Bidimensional duct assumed for test rigs acoustic model: (1) upstream section; (2) lined section with impedance Z, and (3) downstream section. Acoustic waves propagate either upstream or downstream the flow. An uniform flow with Mach number M is assumed.

1. Convected Helmholtz Equation Method (CHE)

A complete description of the CHE method is provided by Watson et al. [15]. It consists of using a finite element method (FEM) approach to solve the boundary value problem defined in Eqs. (1–6). The impedance Z is then educed by minimizing the objective function

$$F(Z) = \frac{1}{N}\sum_{j=1}^{N}\left|p(z_j)_{\text{num}} - p(z_j)_{\text{exp}}\right| \tag{7}$$

where N is the number of upper-wall microphones, z_j is the axial location of the jth microphone, "num" denotes the numerical values obtained from the FEM, and "exp" denotes the experimental measured values.

2. Mode-Matching Method

To avoid the computational cost of the FEM model to determine the theoretical field, one can use an analytical model of the acoustic propagation. For instance, Elnady et al. [11] proposed to use a mode-matching (MM) method to determine the acoustic field. The MM method consists of using the modal structure of the acoustic field to compute the numerical solution. The MM method is summarized in this work, and more details of the method can be found in Spillere et al. [4]. We can rewrite the convected Helmholtz equation in a suitable form to solve it as a generalized eigenvalue problem. This problem is solved using a pseudospectral method, and the modal amplitudes can be determined by matching acoustic mass and momentum at each interface. An initial guess for the impedance is considered, and the actual impedance is then found by minimizing the cost function given by

$$\mathcal{F}(Z) = \sum_{j=1}^{N}\left|\frac{p(z_j)_{\text{exp}} - p(z_j)_{\text{num}}}{p(z_j)_{\text{exp}}}\right| \tag{8}$$

which compares the numerical acoustic field computed and the measured acoustic field. One may notice that the cost functions defined by Eqs. (7) and (8) are similar but not identical. These differences should have minimal impact on the conclusions.

3. Kumaresan and Tufts Method (KT)

In order to extract the axial wavenumber and under the assumption of an infinitely long duct, one can use Prony-like algorithms to fit a sum of damped complex exponentials to the measured acoustic pressure at uniformly spaced locations [14]. Once the axial wavenumber is known, it is straightforward to calculate the liner impedance by solving the system of equations obtained from Eqs. (5) and (6). In this case, the acoustic pressure at the flush-mounted microphones at the wall opposite to the liner sample is given by

$$p_j = \sum_{n=1}^{\mathcal{N}} A_n \exp\left(-\mathrm{i}k_{z,nj}j\Delta z\right) + w_j \quad \text{for } j = 0,\ldots,\mathcal{M}-1 \tag{9}$$

where p_j represents the pressure at the jth microphone, Δz is the distance between two consecutive microphones, w_j is the measurement noise, $\mathcal{M}$ is the number of microphones, and $\mathcal{N}$ the number of modes used, in this case 6.

One main issue of using the original Prony's algorithm, as proposed for use in impedance eduction by Jing et al. [14], is its poor performance in the presence of noise w_j [12]. As an alternative, the Kumaresan and Tufts (KT) algorithm [12] has been successfully applied [10,19], providing lower uncertainty levels by selecting a reduced number of wavenumbers (propagating modes) [20]. In this work, the KT algorithm will be used by both institutions to extract the axial wavenumbers from measured acoustic fields, but with different strategies to select the wavenumbers.

The UFSC team selects the least attenuated mode, which is normally associated with the mode containing the most power [20]. On the other hand, the NASA Langley team takes advantage of the higher number of microphones, which allows a higher number of extracted wavenumbers, and initially selects the six lowest-order modes. An interactive process is then applied, following the sequence as follows: i) compute the impedance from each mode, ii) use that impedance to compute the sound field, and iii) select the impedance/mode that minimizes the difference between the computed and measured sound fields.

B. UFSC Liner Impedance Test Rig

The UFSC Liner Impedance Test Rig is a grazing flow acoustic impedance facility located at the Laboratory of Vibration and Acoustics of the Federal University of Santa Catarina, Brazil. A three-dimensional schematic view of the test rig is shown in Fig. 2. The test rig is composed of modular, rectangular-cross-sectioned 40 mm × 100 mm ducts. Quasi-anechoic terminations at the test rig inlet and outlet minimize acoustic reflections. Eight compression drivers are distributed both upstream and downstream of the liner test sample holder to generate sound fields up to 150 dB propagating with or against the flow. Grazing flow is supplied by an external compressed air system, capable of providing a cross-section-averaged flow up to Mach 0.7. A differential pressure transmitter is connected to a 2-mm-diameter Pitot tube located at the test rig inlet.

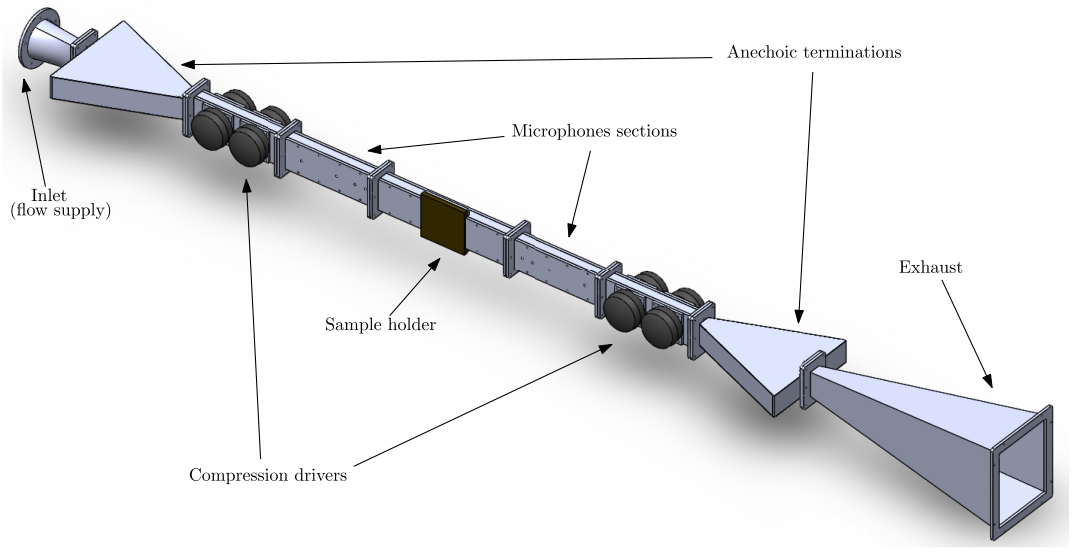

Fig. 2 Schematic representation of the UFSC Liner Impedance Test Rig.

This Pitot tube is used to control the flow average speed at the test section by using a precalibrated factor based on comparisons between the centerline Mach number in the inlet and the bulk Mach number at the test section. Temperature is monitored with a temperature transmitter at the test rig inlet.

An array of eight equally spaced, flush-mounted microphones is located on the wall opposite to the liner section for impedance eduction. Signals are recorded using a data acquisition (DAQ) module at a sampling rate of 25.6 kHz. Measurements are performed using a harmonic excitation signal, which also serves as a reference for cross-spectrum estimation using Welch's method with 30 averages of 25,600 samples with 75% overlap. An in-house Python3 code is used for all hardware control, signal processing, and postprocessing of the data.

C. NASA Grazing Flow Impedance Tube

The NASA Langley GFIT facility is used to measure the acoustic characteristics of noise reduction treatments (acoustic liners) for aircraft jet engine nacelles and nozzles. The facility is a wind tunnel with a rectangular cross-section of 50.8 mm × 63.5 mm, as depicted schematically in Fig. 3. The flow path consists of a straight duct with an upstream acoustic source section using 12 drivers, interchangeable lengths of blank duct, a test section where the liner sample is held along the upper wall of the duct, and an array of 95 measurement microphones leading to a six-driver downstream source section. Near-anechoic terminating diffusers are employed at each end of the duct to control reflections and reduce overall flow noise. The source sections can generate sound pressure levels up to 150 dB for the frequency range between 400 and 3000 Hz. In the current work, swept-sine excitation is used to cover the desired frequency range [21]. To generate the desired flow conditions, pressurized and heated air is supplied to the inlet of the GFIT, while a vacuum system is employed at the duct exit to evacuate air from the tube. With this arrangement, static pressure at the test section can be held to near-ambient conditions at all flow velocities with constant total temperature. Grazing flow Mach numbers from 0 to 0.6 are available with such an arrangement.

D. Semiempirical Liner Impedance Model

The Goodrich liner impedance model proposed by Yu et al. [16] is used as a reference for the comparison of the results between test rigs and to evaluate the impact of different flow profiles. The basic equation of the model is given by

$$Z = Z_{\text{of}} + S_r U_0 + R_{\text{cm}} + \text{i}\left(S_m U_0 - \cot(kh)\right) \tag{10}$$

where Z_{of} is the perforate plate impedance, S_r is the nonlinear resistance slope, R_{cm} is the normalized grazing flow-induced acoustic resistance, S_m is the nonlinear mass reactance, h is the liner cavity height, and U_0 is the root-mean-squared acoustic particle velocity. In this work, U_0 is obtained by solving $Z = p_{\text{ref}}/U_0$ in Eq. (10), with $p_{\text{ref}} = 20\ \mu\text{Pa} \cdot 10^{\text{SPL}_{\text{ref}}/20}$, where the reference SPL SPL_{ref} is the same for both facilities.

The perforated plate impedance is given by

$$Z_{\text{of}} = \text{i}\omega \frac{(t + \varepsilon d)}{c_0 \sigma F\left(\frac{k_s d}{2}\right)} \tag{11}$$

where t is the facesheet thickness, d is the perforated plate hole diameter, σ is the percentage of open area, $F(k_s d/2)$ is the cross-section-averaged hole velocity profile from Crandall's solution [22], and

$$\varepsilon d = \frac{d(1 - 0.7\sqrt{\sigma})}{1 + 305M^3} \tag{12}$$

is the effective mass end correction [23]. The cross-section-averaged hole velocity profile is defined as

$$F\left(\frac{k_s d}{2}\right) = 1 - \frac{2J_1\left(\frac{k_s d}{2}\right)}{\frac{k_s d}{2} J_0\left(\frac{k_s d}{2}\right)} \tag{13}$$

where J_0 and J_1 are zero- and first-order Bessel functions, and

$$k_s^2 = -\text{i}\frac{\omega \rho_0}{\mu} \tag{14}$$

is the wavenumber of a viscous Stokes wave and μ the air viscosity.

The nonlinear resistance slope is given by

$$S_r = 1.336541\left(\frac{1 - \sigma^2}{2c_0 C_d^2 \sigma^2}\right) \tag{15}$$

where C_d is the discharge coefficient, which for $t/d \leq 1$ is given by

$$C_d = 0.80695 \sqrt{\frac{\sigma^{0.1}}{\exp\left(\frac{-0.5072t}{d}\right)}} \tag{16}$$

One may notice that this expression for the discharge coefficient was best-fitted for orifices with perfectly sharp edges, which is not the case in this work, where rounding is expected due to the liner sample manufacturing process. However, for the purpose of this work, the nonlinear resistance contribution induced by the grazing flow is the variable of interest, and this minor divergence in the discharge coefficient becomes negligible.

The normalized acoustic resistance under grazing flow is given by the Rice–Heidelberg derivation [24], such that

$$R_{\text{cm}} = \frac{M}{\sigma\left(2 + 1.256\frac{\delta^*}{d}\right)} \tag{17}$$

where δ^* is the flow profile boundary-layer displacement thickness (BLDT). Finally, the nonlinear mass reactance is given by

$$S_m = -0.0000207\frac{k}{\sigma^2} \tag{18}$$

For the 3D-printed liner sample tested in this work, the thickness of the wall between two honeycomb cells is significant when compared to the active area of the cavity. Jones and Nark [25] considered that the partition wall may lead to a blockage effect in this type of sample and added these effects to a semiempirical model, which resulted in a better agreement with experiments. In the present work, the Goodrich semiempirical model was adapted to

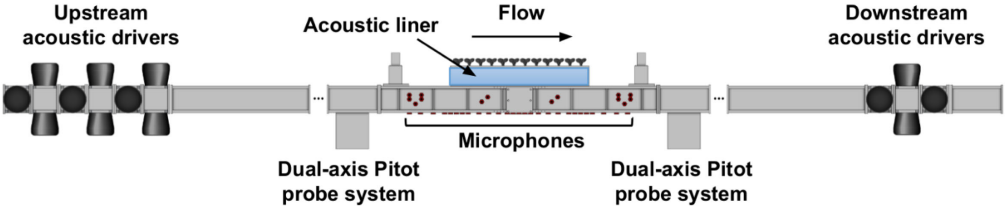

Fig. 3 Schematic representation of the NASA Langley Research Center Grazing Flow Impedance Tube (GFIT).

account for such effects following a similar approach where the backing impedance is replaced by a calculated core impedance. The sequence adopted was to calculate the impedance of the liner core, add the blockage effects, and then add the perforated facesheet impedance. The sequence is slightly different than the one reported by Jones and Nark [25].

The first step is to calculate the impedance of the core of the liner sample. This was done by means of the Zwikker and Kosten transmission line (ZKTL) model, which computes the acoustic pressure and the particle velocity in the core as described in Jones and Nark [25]. The backplate acoustic pressure p_0 and particle velocity U_0 are considered 1 and 0, respectively. The ZKTL model computes changes between the backplate and the core as

$$\begin{pmatrix} p_1 \\ u_1 \end{pmatrix} = \begin{pmatrix} \cosh(k\Gamma h) & Z_c \sinh(k\Gamma h) \\ Z_c^{-1} \sinh(k\Gamma h) & \cosh(k\Gamma h) \end{pmatrix} \begin{pmatrix} p_0 \\ u_0 \end{pmatrix} \tag{19}$$

where the propagation constant Γ and characteristic impedance Z_c within the empty chamber are calculated as

$$\Gamma = \sqrt{\frac{J_0(\mathrm{i}^{3/2}s)}{J_2(\mathrm{i}^{3/2}s)}}\sqrt{\frac{\gamma}{n_\Gamma}} \quad \text{and} \quad Z_c = \frac{-\mathrm{i}}{\Gamma}\frac{J_0(\mathrm{i}^{3/2}s)}{J_2(\mathrm{i}^{3/2}s)} \tag{20}$$

and

$$s = (d_c/2)\sqrt{\rho\omega/\mu} \quad \text{and} \quad n_\Gamma = \left[1 + \frac{\gamma - 1}{\gamma}\frac{J_2(\mathrm{i}^{3/2}P_n^{1/2}s)}{J_0(\mathrm{i}^{3/2}P_n^{1/2}s)}\right]^{-1} \tag{21}$$

where $\gamma = 1.4$ is the heat capacity ratio, d_c is the chamber dimension, and P_n is the Prandtl number.

After obtaining the acoustic pressure and the particle velocity, the core impedance can be directly obtained. The partition wall effect is then included by

$$Z_b = \frac{p_1}{u_1}\frac{A_t}{A_a} \tag{22}$$

where Z_b is the core impedance considering the blockage effect, A_a is the active area of the cavity, and A_t is the total area, which includes the partition thickness.

Finally, the Goodrich semiempirical model, Eq. (10), is then adjusted by substituting the $-\cot(kh)$ term with the impedance obtained for the core with the blockage effect, resulting in

$$Z = Z_{\mathrm{of}} + S_r U_0 + R_{\mathrm{cm}} + \mathrm{i}(S_m u_0) + Z_b \tag{23}$$

E. Liner Samples and Test Matrix

For the purpose of this work, two liner samples were manufactured via stereolithography additive manufacturing. The liner samples were designed as arrays of individual 9.9 mm × 9.9 mm square chambers with chamber heights of $h = 38.1$ mm. Each chamber contains eight holes with a diameter $d = 0.99$ mm, resulting in a single-chamber percentage of open area of 6.3%. The design facesheet thickness is $t = 0.635$ mm. The design cell walls are 2.54 mm thick, resulting in an overall percentage of open area of 4.2%. Each sample was arranged to fit the different sample holders for each test rig. The UFSC sample consists of an array of 8×33 cells, while the NASA sample is 4×44. Since the liner samples were not printed with an integrated backplate, a 6.35-mm-thick aluminum plate was used for this purpose. The UFSC sample can be seen in Fig. 4.

The liner samples used at UFSC and NASA were 3D-scanned, and the results are presented in the Appendix. Some differences between the nominal and the actual liner geometry were observed. Small differences, attributed to the manufacturing procedure, were also found between the two samples. In the following analysis, the scanned geometry of each liner sample is used as an input parameter for the semiempirical model, together with the flow characteristics. However, the effects on impedance caused by the geometries are not discussed in detail since the effects of flow profile are the main focus of this work. A detailed analysis of the impact of the geometric differences will be the subject of future publications.

Tests were conducted under four different flow conditions at both test rigs: i) in the absence of flow, ii) at a centerline Mach number of $M_{\mathrm{center}} = 0.3$, iii) at a centerline Mach numbers of $M_{\mathrm{center}} = 0.5$, and iv) at an average Mach number of $M_{\mathrm{avg}} = 0.265$.

For the UFSC test rig, a stepped pure tone excitation was used in a frequency range from 500 to 2500 Hz with 100 Hz steps, while the

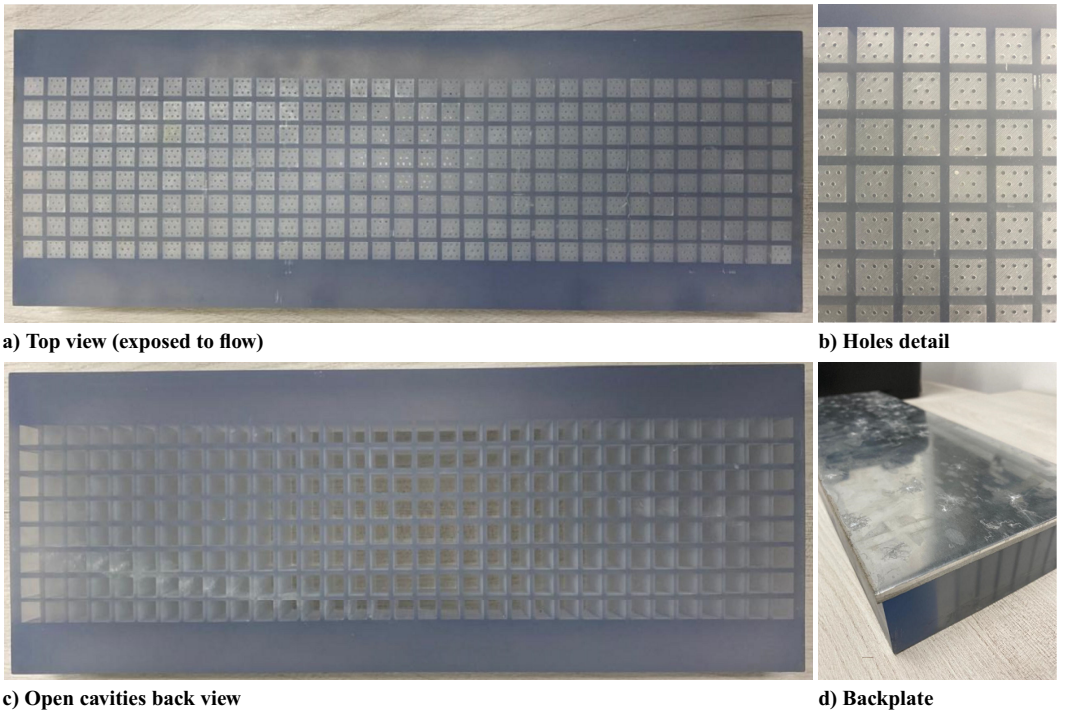

a) Top view (exposed to flow) **b) Holes detail**

c) Open cavities back view **d) Backplate**

Fig. 4 Pictures from UFSC test sample.

NASA team used a swept sine with a 10 Hz resolution in the same frequency range. Tests were conducted in both test rigs at SPLs of 130 and 145 dB. However, these source levels were set differently in the two rigs. For the UFSC test rig, the source level set point SPL is the incident plane wave amplitude, whereas NASA uses the total SPL at the edge of the liner closest to the acoustic source that is engaged. As a result, the liner in the NASA GFIT will experience a different sound field (frequency dependent) from that used in the UFSC test rig. This difference will affect the comparison of results between the two test rigs. However, since the test liner is weakly nonlinear (and therefore weakly dependent on source SPL), these differences should be limited over the majority of the frequency range of interest.

III. Results and Discussion

A. Flow Profiles

This section presents the flow profiles measured for both test rigs at centerline Mach numbers of 0.3 and 0.5. The description of the NASA measurements can be found in Jones et al. [26]. For the UFSC flow profile, the measurements were conducted with a 0.63-mm-diameter Pitot tube at the liner sample's upstream edge position. Measurements were taken with a 1 mm step increment. The flow profiles are presented in Fig. 5. Both flow profiles are normalized by the centerline Mach number, which shows very similar trends between the lower and higher Mach numbers. The BLDT δ^* for both test rigs were determined from the centerline (1D profile) measured data (linear extrapolation to the wall). The BLDT is given by

$$\delta^* = \int_0^H \left(1 - \frac{u(x)}{U_\infty}\right) \mathrm{d}x \tag{24}$$

where $u(x)$ is the local velocity within the boundary layer, and U_∞ is the freestream velocity, which for this case corresponds to the centerline velocity. Since we are interested in the effect of the boundary layer over the lined wall, the BLDT will be evaluated in the present work over the half channel height on the liner sample side. Due to instrumentation limitations at UFSC, measurements were performed only at the upstream liner edge (leading edge). Measurements across the duct cross-section (2D profile) were also conducted to determine the bulk Mach number, which is calculated using a quadrature method average [27] with a 5×5 point grid. Table 1 presents the flow parameters calculated for each facility for both centerline Mach numbers. In the following sections, the BLDT and bulk Mach number results will be used to evaluate the impact of the flow profile on the liner impedance.

Table 1 Flow parameters

	$M_c = 0.3$		$M_c = 0.5$	
Facility	δ^*, mm	Bulk Mach	δ^*, mm	Bulk Mach
UFSC	1.9	0.265	2.0	0.442
NASA	3.3	0.238	3.4	0.372

B. Acoustic Results

In this section, the impedances educed in both test rigs are compared. The MM and KT methods are used to postprocess data collected at the UFSC test rig, while the CHE and KT methods are employed to analyze data collected at the NASA GFIT. The experimental results are also compared with the predictions from the Goodrich semiempirical model for each test rig. In the first approach, the test rigs were set to match the same maximum Mach number (centerline Mach number) in the cross-section, resulting in slightly different bulk Mach numbers.

The results obtained with both test rigs at 130 dB in the absence of mean flow are presented in Fig. 6. Overall, a very good agreement is observed between experimental results. This is especially true in the frequency range with higher acoustic attenuation, where the experimental uncertainties are expected to be low [20]. The discrepancy in the resistance slope observed at lower frequencies may be explained by the low attenuation level and/or the reduced liner length-to-wavelength ratio [28]. The semi-empirical model displays a hump in the resistance close to the liner's first resonance frequency (around 1600 Hz), which is not observed in the experimental data. This behavior may be due to the model overestimating the nonlinear characteristics of the liner, which are typically characterized by such a hump. The reactance obtained by the semiempirical model shows good agreement with the experimental results. However, near the liner resonance, the experimental results display a reasonable divergence from the model. This can be explained by the fact that the model is adjusted for a single value of SPL, while a decay is expected along the sample. Also, we should keep in mind that the Goodrich model has been tuned based on impedance results from the in-situ method and considering traditional liners, which generally display sharp edges in holes, while we are considering a 3D-printed sample with rounded edges in the holes. The agreement between the results of each test rig for the case without flow provides confidence in the manufacturing process and the similarity of the samples, enabling further comparisons for the cases with grazing flow.

Figures 7a and 7b show the experimental results obtained with both test rigs at 130 dB and for both propagation directions at a centerline Mach number of 0.3. The results follow the expected pattern, where the resistance increases with the presence of grazing flow when compared with the results without flow in Fig. 6. Additionally, the

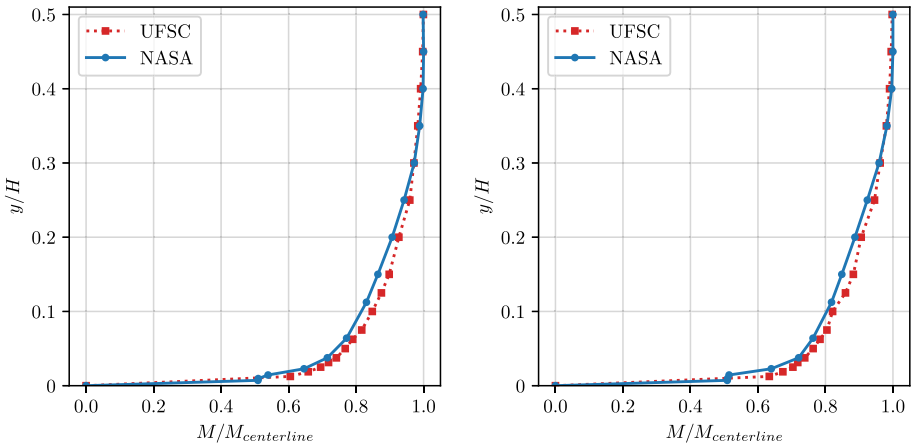

a) Centerline Mach number of 0.3 b) Centerline Mach number of 0.5

Fig. 5 Flow profiles obtained for each test rig.

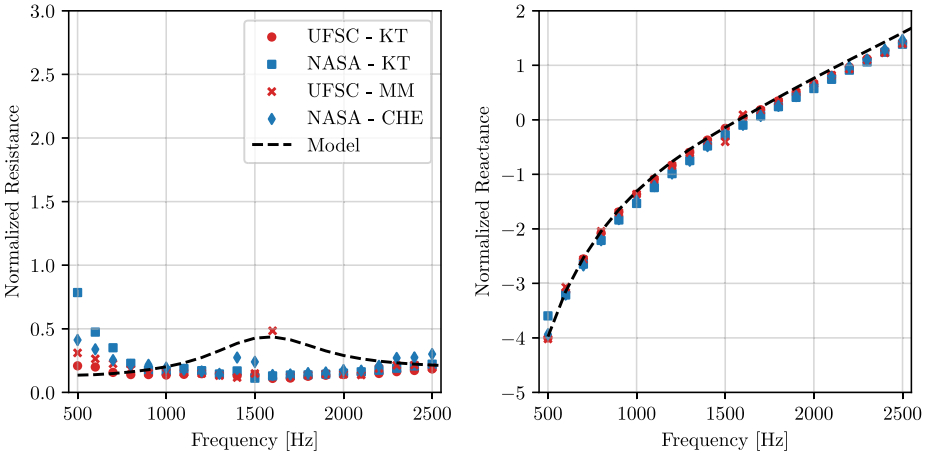

Fig. 6 Educed impedances in absence of flow and at 130 dB.

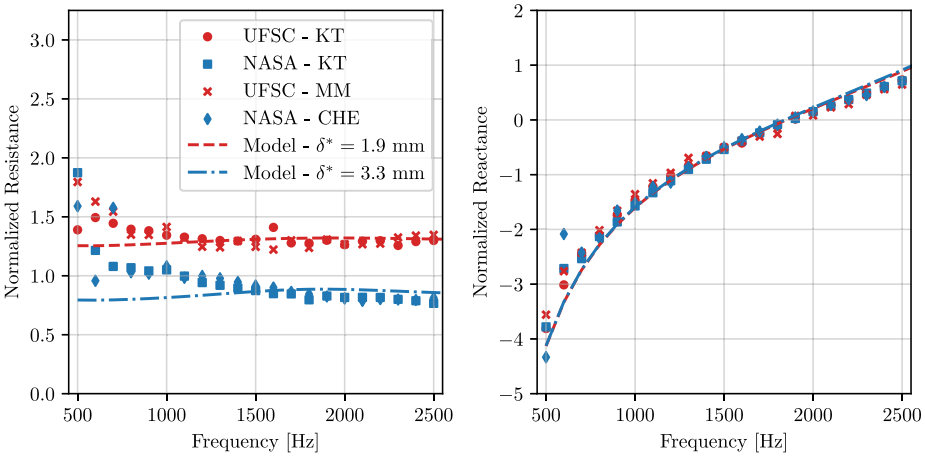

a) Upstream source

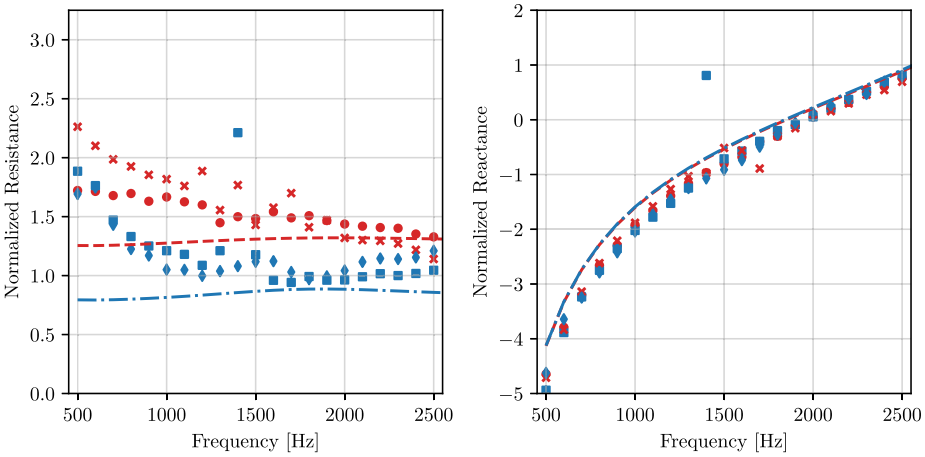

b) Downstream source

Fig. 7 Educed impedances with centerline Mach number 0.3 at 130 dB.

results obtained with both test rigs exhibit the differences reported in the literature between upstream and downstream acoustic source configurations. These differences are still under debate in the community, whether as a failure of the Ingard–Myers boundary condition or an inherent part of liner physics [4,10,29]. Despite the very good agreement observed in the educed reactance, the acoustic resistance measured within the UFSC facility is consistently higher than the one measured in the NASA GFIT. As mentioned earlier, the flow profile is expected to affect the liner resistance [6], and the differences in the bulk Mach number and the BLDT reported in Sec. III.A may be a possible source of discrepancies. There are—at least—two possible sources for the discrepancies found in the acoustic impedance: I) interactions between the acoustic field and the different boundary layers are resulting in different impedances for the two facilities, or II) the uniform flow approximation assumed in the inverse methods is introducing a bias error in the acoustic field modeling, which is different for each facility. In this work, we will initially consider the first hypothesis, based on the early work of Hersch and Walker [30]. They conducted an experimental campaign specially designed to investigate the impact of the flow profile on the discharge coefficient of an orifice with an incident normal acoustic wave. Since their work did not rely on any uniform flow assumption,

their findings provide a strong basis for the first hypothesis discussed here that the differences in the impedance may arise physically and independently from the uniform flow simplification.

To assess the potential impact of the different flow profiles measured at each test rig, Figs. 7a and 7b also include the impedances obtained using the semiempirical model presented in Sec. II.D. The main differences in the prediction inputs are the BLDT and the bulk Mach number measured at each test rig. The semiempirical model predictions for both geometries closely match the differences observed in the resistance between the results from each test rig, suggesting that the flow profile plays a significant role in the eduction process. Indeed, one may notice that a smaller δ^* results in a higher resistance. A thinner BLDT indicates a higher velocity gradient near the wall and, therefore, a high velocity near the orifices. Some studies have shown that the grazing flow interacts with the orifices, creating a recirculation area inside the holes that reduces the discharge coefficient. The strength of the recirculation vortex depends on the velocity gradient, which in turn can affect the discharge coefficient [31–33].

The results for 130 dB and both source positions at a centerline Mach number of 0.5 are presented in Figs. 8a and 8b. As expected, the increase in the grazing flow Mach number results in higher resistance. The higher Mach number also leads to more oscillations and outliers in the results due to lower signal-to-noise ratio (SNR) in the measurements. The mode-matching method is more sensitive to this, which is observed in the difference in the impedances educed by each method at the UFSC facility. In general, the same trend observed for Mach number 0.3 is also seen for Mach number 0.5. A good match is observed for the reactance results between different test rigs, but the educed resistance is consistently higher at the UFSC test rig when compared to the NASA GFIT for most of the frequency range. The discrepancy between upstream and downstream sources can also be observed, and it is more pronounced in the UFSC facility. The results for the semiempirical model are also included in Figs. 8a and 8b. Once more, the model correctly captures the impact of different flow profiles on the resistance, corroborating the hypothesis that the difference in displacement thicknesses can be used to account for the discrepancies between the impedance educed at each test rig. It may also be noted that the results from the semi-empirical model display a better match to the upstream source results (downstream propagation). From this point, for the sake of brevity, only results obtained with an upstream acoustic source are going to be shown.

Although differences in displacement thickness may account for different impedance results, an alternate hypothesis is that differences in bulk Mach number are responsible for test rig differences. Indeed, when matching the centerline Mach number between test rigs, the bulk Mach numbers are different. To assess the sensitivity of the semiempirical model to both the flow profile (characterized by the BLDT δ^*) and the average Mach number, a parametric analysis was conducted. The results of this analysis are depicted in Fig. 9, and they clearly indicate that when the same average Mach number is used in both facilities, the primary factor influencing the impedance differences is the flow profile, especially under the specified conditions of the test rigs.

To validate some of the conclusions drawn from the parametric analysis, a new set of tests was conducted at the NASA GFIT test rig. In this case, the flow velocity was adjusted to match the same average Mach number as observed at the UFSC test rig, $M_{\text{avg}} = 0.265$. The results of this comparison are presented in Fig. 10. It is evident that the results exhibit a very similar discrepancy to that observed in Fig. 7 for the case with the same centerline Mach number. These differences correlate well with those predicted for the measured differences in displacement thickness between the two

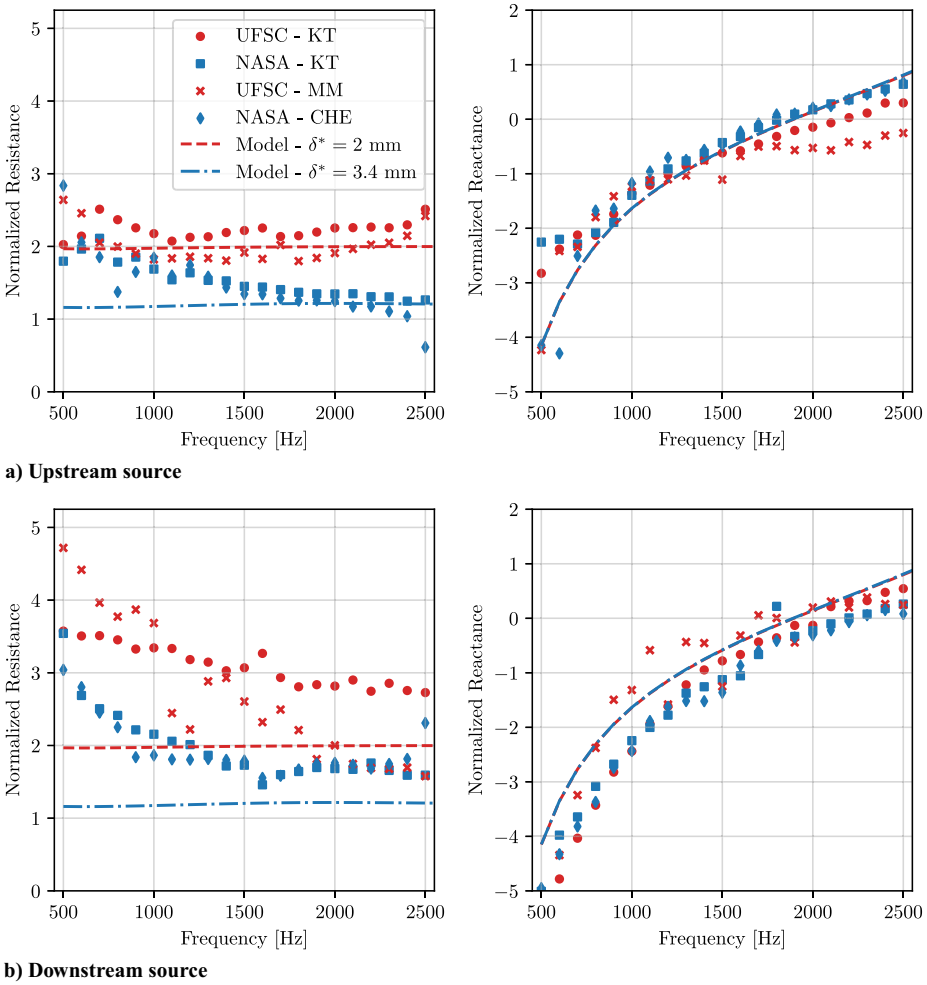

Fig. 8 Educed impedances with centerline Mach number 0.5 at 130 dB.

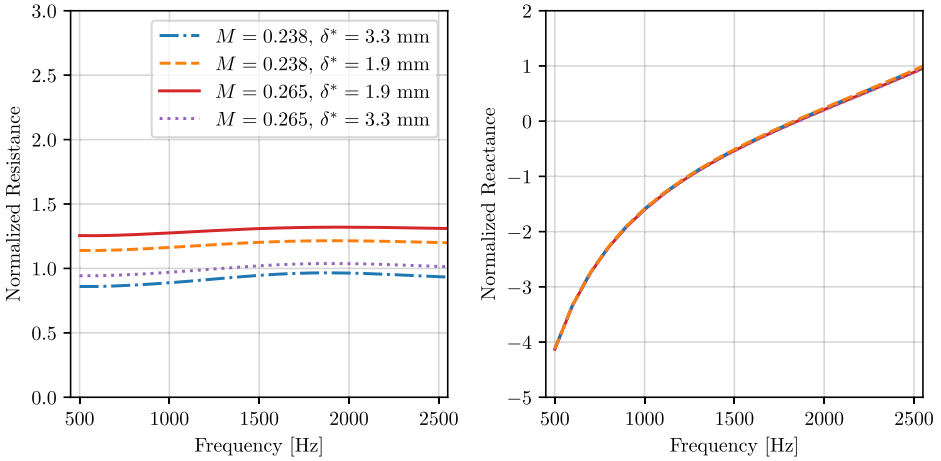

Fig. 9 Parametric analysis performed with the Goodrich semiempirical model. $M = 0.265$ and $\delta^* = 1.02$ mm correspond to UFSC data, and $M = 0.238$ and $\delta^* = 2.60$ mm to GFIT flow profile measurements.

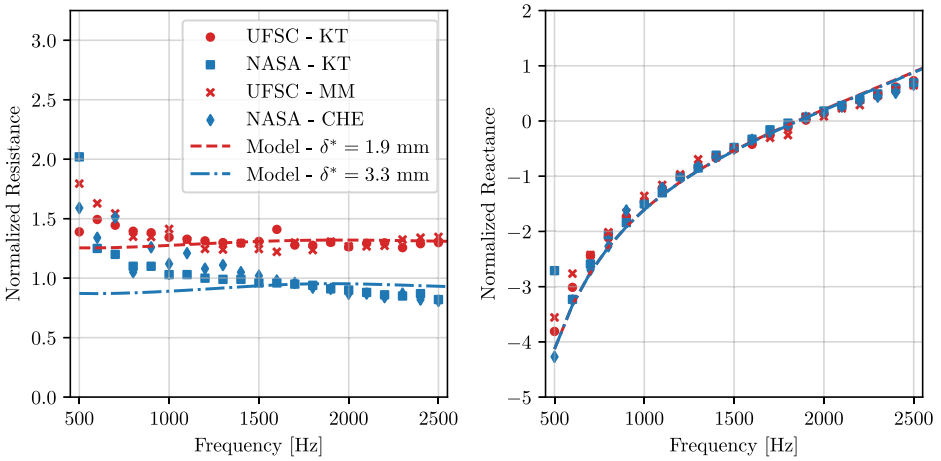

Fig. 10 Educed impedances with same mean flow Mach number 0.265 and at 130 dB in both test rigs. Upstream source.

test rigs. They also highlight the importance of accurately characterizing the flow profile in a test rig and considering it when comparing impedance results between different test rigs.

In a final step to verify the procedures at each facility, a cross-check of the algorithms was performed. It is known that different eduction methods and algorithms may lead to small differences in the educed impedance, even with data collected within the same test rig [28]. For this purpose, both teams shared their raw acoustic pressure data and all other necessary parameters for the eduction process (e.g., Mach number, temperature, detailed geometric dimensions of the test rig). NASA's data was used for this comparison due to the longer liner sample and higher number of microphones, which provide lower uncertainties with Prony-like methods [20]. The comparison included both acoustic source locations and centerline Mach numbers of 0.0 (no flow), 0.3, and 0.5. The results obtained for the KT algorithms are presented in Fig. 11. The comparison between the MM and CHE methods is shown in Fig. 12.

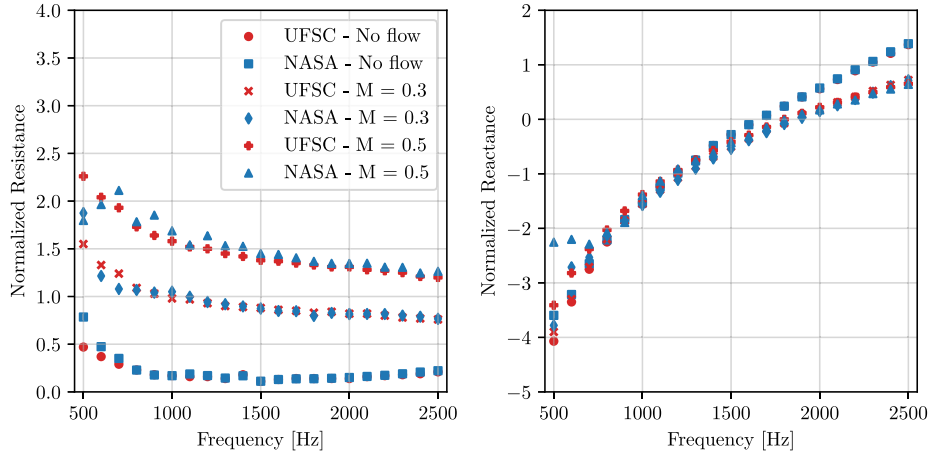

Fig. 11 Educed impedances with NASA data postprocessed by UFSC and NASA for the three centerline Mach numbers and at 130 dB for the KT algorithms. Upstream source.

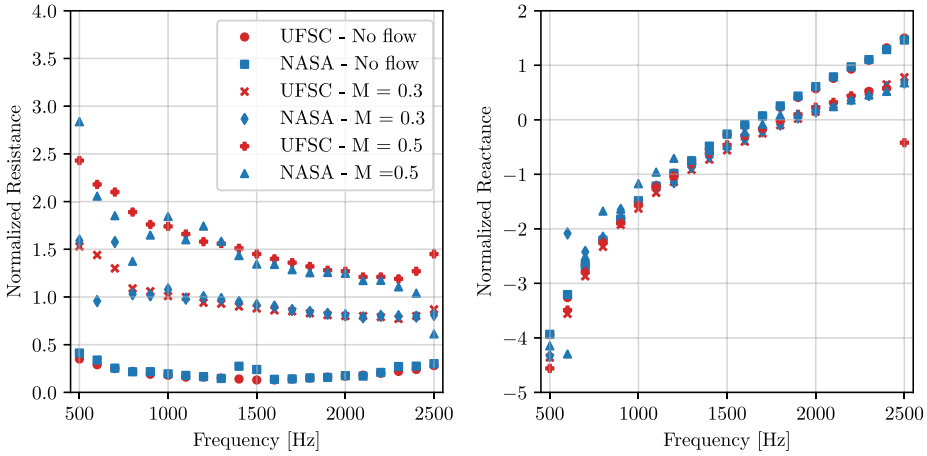

Fig. 12 Educed impedances with NASA data postprocessed by UFSC and NASA for the three centerline Mach numbers and at 130 dB for the MM and CHE methods. Upstream source.

As expected, the comparison of educed impedances using the same dataset presented an almost perfect match, especially when utilizing the KT method as implemented by each institution. Small differences were observed with higher Mach numbers and downstream source configurations, which could be attributed to the mode selection process leading to slight discrepancies in the educed impedance [20]. Slightly larger differences were observed when comparing the MM and CHE methods, which is understandable given that these methods are quite distinct. Overall, good agreement was still observed for these methods. This analysis further corroborates that the previously observed differences in impedance results may indeed be attributed to the different flow profiles of the test rigs. The educed impedances for 145 dB for all the configurations tested displayed similar trends with the results for 130 dB. For the sake of brevity, only results with 130 dB are presented in this work.

IV. Conclusions

This paper presented a comprehensive comparison of impedance results obtained using two different impedance eduction test rigs for the same acoustic liner. The study aimed to investigate the factors contributing to variations in impedance measurements across different facilities. Two liner samples were manufactured using 3D printing technology to minimize manufacturing-induced errors. The two samples were 3D scanned and compared. Despite the best effort in using the same manufacturer and printer, small differences were found. One sample was tested at the NASA Langley GFIT, while the other was tested at the UFSC Liner Test Rig. Initial tests conducted at both facilities under no-flow conditions demonstrated a high degree of similarity in the educed impedance, confirming the close similarity of the samples. This suggests that the impact of the geometrical differences is negligible in the absence of flow. Subsequent tests involved matching the centerline Mach number between the test rigs. Surprisingly, the results obtained at UFSC showed significantly higher acoustic resistances than those observed at the NASA Langley GFIT in the presence of grazing flow. A semiempirical model was employed to identify the key parameter affecting the impedance results, and the BLDT δ^* was identified as the primary source of discrepancies, considering that in the absence of flow, the two samples provided very similar results. To further investigate this, tests were conducted at NASA's GFIT, targeting an average Mach number matching that of the UFSC test rig. Remarkably, the new results exhibited the same pattern of discrepancies, supporting the conclusion that differences in flow profiles between the test rigs are responsible for the higher acoustic resistances observed at UFSC. To ensure the robustness of the impedance measurement methods, a cross-comparison of eduction algorithms was conducted by sharing raw data obtained by NASA with the UFSC team. The results of this comparison revealed no significant differences in the educed impedance values using different methods, supporting the hypothesis that differences in flow profiles are the primary cause of impedance variations. The results presented in this study emphasize the critical role of accurately characterizing and reporting the flow profile in a test rig and taking it into account when comparing impedance results between different test rigs. This factor significantly impacts the educed acoustic impedance, particularly the acoustic resistance, and can lead to variations in the results obtained from different facilities. Understanding and quantifying the flow profile is crucial for ensuring the reliability and comparability of impedance measurements across different test setups. It is finally worth mentioning that the impact of the small differences between the two samples will be investigated in future studies.

Appendix: Scanned Geometry

The liner samples, tested at UFSC and NASA, were 3D scanned at both institutions with different hardware. The hardware used at UFSC allowed spatial resolution of 0.01 mm, while the one at NASA of 0.04 mm. This was done in order to compare the manufactured geometries against the nominal one. A 3D view of the liner

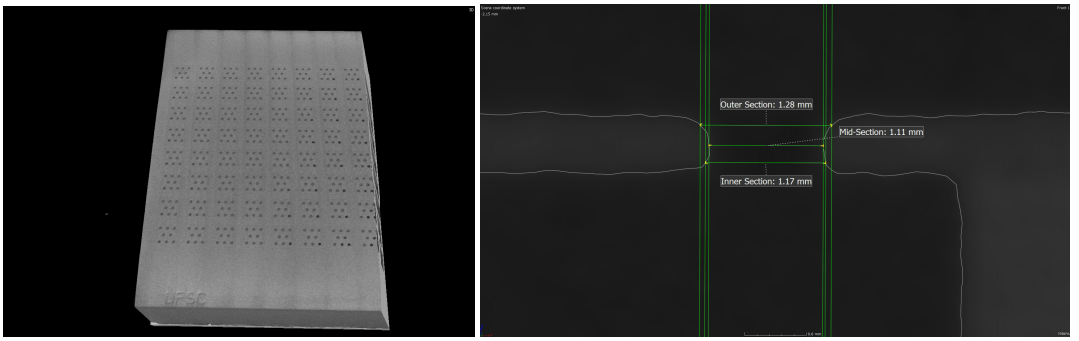

a) Overview of the liner scan **b) Measurements of the hole diameter and shape**

Fig. A1 Liner sample scan.

Table A1 Design and measured geometry parameters

Parameter	Design	Measured (UFSC)	Standard deviation (UFSC)	Measured (NASA)	Standard deviation (NASA)
Facesheet thickness, mm	0.635	0.55	0.03	0.61	0.03
Hole diameter, mm	0.99	1.17	0.06	1.21	0.06
POA	4.2%	5.7%	— —	6.3%	— —
Rounding radius, mm	— —	0.066	0.03	0.085	0.08

scanned at UFSC and a detailed view of one of the orifices, with measurements, are shown in Fig. A1. Other parameters were evaluated: facesheet thickness and the shape of the orifices.

The quantitative comparison between the two samples is summarized in Table A1. Geometrical parameters were obtained by averaging measurements taken over different cavities. The standard deviation represents the variability between the different sampling locations. It is evident that for both samples the measured facesheet thickness was smaller than the design value, while the opposite is found for the hole diameter. This latter caused the percentage of open area (POA) to be larger than the design value. Furthermore, the edges of the orifices are not sharp but rounded.

When comparing the two samples, there are small differences in terms of both mean facesheet thickness and hole diameter. Despite the best effort made to manufacture the same samples, still differences are present. The fact that in the absence of flow the two samples provided similar impedance values suggests that the impact of the geometrical differences is not large. However, future studies will investigate this aspect in greater depth.

Acknowledgments

L.A.B., N.T.Q., and J.A.C. gratefully acknowledge funding support from Funding Authority for Studies and Projects (FINEP), National Council for Scientific and Technological Development (CNPq), and EMBRAER S.A. L.A.B. and N.T.Q. acknowledge scholarships from the Coordenação de Aperfeiçoamento de Pessoal de Nível Superior—Brasil (CAPES). N.T.Q., L.A.B., and J.A.C. acknowledge Lucas M. Pereira (UFSC) and Andrey R. da Silva (UFSC) for the help during the measurements and discussions. The work of F.A. is cofunded by the European Union (ERC, LINING, 101075903). Views and opinions expressed are, however, those of the author(s) only and do not necessarily reflect those of the European Union or the European Research Council. Neither the European Union nor the granting authority can be held responsible for them. M.G.J., B.M.H., and D.M.N. acknowledge Martha Brown and Alonzo (Max) Reid for assistance in gathering data in the GFIT. This work was conducted in support of Advanced Air Transport Technology Project. This work was partially supported by the AeroAcoustics Research Consortium (AARC). The AARC is a government–industry partnership supporting precompetitive research for aircraft noise reduction. The authors gratefully acknowledge Fundação CERTI (Reference Centers for Innovative Technologies) for carrying out the scanning of the sample as part of an institutional collaboration with UFSC.

References

[1] Kuropatwa, M., Wegrzyn, N., and Kozuba, J., "Turbofan Engines Efficiency, Historical Trends, and Future Prediction," *Safety & Defense*, Vol. 8, No. 2, 2022, pp. 82–90. https://doi.org/10.37105/sd.186

[2] Jones, M. G., Simon, F., and Roncen, R., "Broadband and Low-Frequency Acoustic Liner Investigations at NASA and ONERA," *AIAA Journal*, Vol. 60, No. 4, 2022, pp. 2481–2500. https://doi.org/10.2514/1.J060862

[3] Bake, F., Burgmayer, R., Schulz, A., Knobloch, K., Enghardt, L., and Jones, M. G., "IFAR Liner Benchmark Challenge #1—DLR Impedance Eduction of Uniform and Axially Segmented Liners and Comparison with NASA Results," *International Journal of Aeroacoustics*, Vol. 20, Nos. 5-7, 2021, pp. 478–496. https://doi.org/10.1177/1475472X211023844

[4] Spillere, A. M. N., Bonomo, L. A., Cordioli, J. A., and Brambley, E. J., "Experimentally Testing Impedance Boundary Conditions for Acoustic Liners with Flow: Beyond Upstream and Downstream," *Journal of Sound and Vibration*, Vol. 489, Dec. 2020, Paper 115676. https://doi.org/10.1016/J.JSV.2020.115676

[5] Roncen, R., Méry, F., Piot, E., and Klotz, P., "Spatially-Varying Impedance Model for Locally Reacting Acoustic Liners at a High Sound Intensity," *Journal of Sound and Vibration*, Vol. 524, April 2022, Paper 116741. https://doi.org/10.1016/j.jsv.2021.116741

[6] Kooi, J., and Sarin, S., "An Experimental Study of the Acoustic Impedance of Helmholtz Resonator Arrays Under a Turbulent Boundary Layer," *7th Aeroacoustics Conference*, AIAA Paper 1981-1998, 1981. https://doi.org/10.2514/6.1981-1998

[7] Jones, M., Tracy, M., Watson, W., and Parrott, T., "Effects of Liner Geometry on Acoustic Impedance," *8th AIAA/CEAS Aeroacoustics Conference & Exhibit*, AIAA Paper 2002-2446, 2002. https://doi.org/10.2514/6.2002-2446

[8] Murray, P., Ferrante, P., and Scofano, A., "Manufacturing Process and Boundary Layer Influences on Perforate Liner Impedance," *11th AIAA/CEAS Aeroacoustics Conference*, AIAA Paper 2005-2849, 2005. https://doi.org/10.2514/6.2005-2849

[9] Murray, P., and Astley, R. J., "Development of a Single Degree of Freedom Perforate Impedance Model Under Grazing Flow and High SPL," *18th AIAA/CEAS Aeroacoustics Conference (33rd AIAA Aeroacoustics Conference)*, AIAA Paper 2012-2294, 2012. https://doi.org/10.2514/6.2012-2294

[10] Renou, Y., and Aurégan, Y., "Failure of the Ingard-Myers Boundary Condition for a Lined Duct: An Experimental Investigation," *Journal of the Acoustical Society of America*, Vol. 130, No. 1, 2011, pp. 52–60. https://doi.org/10.1121/1.3586789

[11] Elnady, T., Bodén, H., and Elhadidi, B., "Validation of an Inverse Semi-Analytical Technique to Educe Liner Impedance," *AIAA Journal*, Vol. 47, No. 12, 2009, pp. 2836–2844. https://doi.org/10.2514/1.41647

[12] Kumaresan, R., and Tufts, D., "Estimating the Parameters of Exponentially Damped Sinusoids and Pole-Zero Modeling in Noise," *IEEE Transactions on Acoustics, Speech, and Signal Processing*, Vol. 30, No. 6, 1982, pp. 833–840. https://doi.org/10.1109/TASSP.1982.1163974

[13] Jones, M. G., Nark, D. M., and Howerton, B. M., "Overview of Liner Activities in Support of the International Forum for Aviation Research," *25 AIAA/CEAS Aeroacoustics 2022 Conference*, AIAA Paper 2019-2599, 2019. https://doi.org/10.2514/6.2019-2599

[14] Jing, X., Peng, S., and Sun, X., "A Straightforward Method for Wall Impedance Eduction in a Flow Duct," *Journal of the Acoustical Society of America*, Vol. 124, No. 1, 2008, pp. 227–234. https://doi.org/10.1121/1.2932256

[15] Watson, W. R., Jones, M. G., and Parrott, T. L., "Validation of an Impedance Eduction Method in Flow," *AIAA Journal*, Vol. 37, No. 7, 1999, pp. 818–824. https://doi.org/10.2514/2.7529

[16] Yu, J., Ruiz, M., and Kwan, H. W., "Validation of Goodrich Perforate Liner Impedance Model Using NASA Langley Test Data," *14th AIAA/CEAS Aeroacoustics Conference (29th AIAA Aeroacoustics Conference)*, AIAA Paper 2008-2930, 2008. https://doi.org/10.2514/6.2008-2930

[17] Ingard, U., "Influence of Fluid Motion Past a Plane Boundary on Sound Reflection, Absorption, and Transmission," *Journal of the Acoustical Society of America*, Vol. 31, No. 7, 1959, pp. 1035–1036. https://doi.org/10.1121/1.1907805

[18] Myers, M., "On the Acoustic Boundary Condition in the Presence of Flow," *Journal of Sound and Vibration*, Vol. 71, No. 3, 1980, pp. 429–434. https://doi.org/10.1016/0022-460X(80)90424-1

[19] Watson, W. R., Carpenter, M. H., and Jones, M. G., "Performance of Kumaresan and Tufts Algorithm in Liner Impedance Eduction with Flow," *AIAA Journal*, Vol. 53, No. 4, 2015, pp. 1091–1102. https://doi.org/10.2514/1.J053705

[20] Bonomo, L. A., Spillere, A. M., and Cordioli, J. A., "Parametric Uncertainty Analysis for Impedance Eduction Based on Prony's Method," *AIAA Journal*, Vol. 58, No. 8, 2020, pp. 3625–3638. https://doi.org/10.2514/1.J059071

[21] Howerton, B. M., Vold, H., and Jones, M. G., "Application of Swept Sine Excitation for Acoustic Impedance Eduction," *25th AIAA/CEAS Aeroacoustics Conference*, AIAA Paper 2019-2487, 2019. https://doi.org/10.2514/6.2019-2487

[22] Crandall, I. B., *Theory of Vibrating Systems and Sound*, Wiley, Hoboken, NJ, 1926.

[23] Rice, E. J., Feiler, C. E., and Acker, L. W., "Acoustic and Aerodynamic Performance of a 6-Foot-Diameter Fan for Turbofan Engines. 3—Performance with Noise Suppressors," NASA TN D-6178, 1971, https://ntrs.nasa.gov/api/citations/19710007779/downloads/19710007779.pdf.

[24] Heidelberg, L., Rice, E., and Homyak, L., "Experimental Evaluation of a Spinning-Mode Acoustic-Treatment Design Concept for Aircraft Inlets," NASA TP 1613, April 1980, https://ntrs.nasa.gov/api/citations/19800012838/downloads/19800012838.pdf.

[25] Jones, M. G., and Nark, D. M., "Partition Thickness Considerations for Additively Manufactured Acoustic Liners," NASA TM 20230013028, 2023, https://ntrs.nasa.gov/api/citations/20230013028/downloads/NASA-TM-20230013028.pdf.

[26] Jones, M. G., Watson, W. R., and Nark, D. M., "Effects of Flow Profile on Educed Acoustic Liner Impedance," *16 AIAA/CEAS Aeroacoustics 2022 Conference*, AIAA Paper 2010-3763, 2010. https://doi.org/10.2514/6.2010-3763

[27] ISO 3966: 2008 - Measurement of Fluid Flow in Closed Conduits—Velocity Area Method Using Pitot Static Tubes, International Organization for Standardization, Genevra, Switzerland, 2008.

[28] Bonomo, L. A., Quintino, N. T., Spillere, A. M., Cordioli, J. A., and Murray, P. B., "A Comparison of In-Situ and Impedance Eduction Experimental Techniques for Acoustic Liners with Grazing Flow and High SPL," *28th AIAA/CEAS Aeroacoustics 2022 Conference*, AIAA Paper 2022-2998, 2022. https://doi.org/10.2514/6.2022-2998

[29] Nark, D. M., Jones, M. G., and Piot, E., "Assessment of Axial Wave Number and Mean Flow Uncertainty on Acoustic Liner Impedance Eduction," *2018 AIAA/CEAS Aeroacoustics Conference*, AIAA Paper 2018-3444, 2018. https://doi.org/10.2514/6.2018-3444

[30] Hersch, A. S., and Walker, B., "Effect of Grazing Flow on the Acoustic Impedance of Helmholtz Resonators Consisting of Single and Clustered Orifices," NASA CR 3177, Aug. 1979.

[31] Zhang, Q., and Bodony, D. J., "Numerical Simulation of Two-Dimensional Acoustic Liners with High-Speed Grazing Flow," *AIAA Journal*, Vol. 49, No. 2, 2011, pp. 365–382. https://doi.org/10.2514/1.J050597

[32] Zhang, Q., and Bodony, D. J., "Numerical Investigation of a Honeycomb Liner Grazed by Laminar and Turbulent Boundary Layers," *Journal of Fluid Mechanics*, Vol. 792, March 2016, pp. 936–980. https://doi.org/10.1017/jfm.2016.79

[33] Avallone, F., Manjunath, P., Ragni, D., and Casalino, D., "Lattice-Boltzmann Very Large Eddy Simulation of a Multi-Orifice Acoustic Liner with Turbulent Grazing Flow," *25th AIAA/CEAS Aeroacoustics Conference*, AIAA Paper 2019-2542, 2019. https://doi.org/10.2514/6.2019-2542

C. Bailly
Associate Editor